

Experimental vs. natural fulgurite: A comparison and implications for the formation process

A. ZEYNEP ÇALIŞKANOĞLU^{1,*†}, CORRADO CIMARELLI¹, DONALD B. DINGWELL¹, AND
ALESSANDRA S.B. CAMARA²

¹Department of Earth and Environmental Sciences, Ludwig-Maximilians-Universität, Theresienstraße 41, 80333 Munich, Germany

²Institute of Energy Systems Munich, Universität der Bundeswehr, Werner-Heisenberg-Weg 39, 85577 Neubiberg, Germany

ABSTRACT

Fulgurites are glassy structures formed when lightning strikes the ground, causing ground material (e.g., rocks, sediments, or soil) to melt and fuse. While fulgurites are relatively rare, they provide valuable insights into paleoecology and may play a key role in prebiotic chemistry. Despite their significance in nature, understanding the conditions underlying the formation of fulgurites poses severe challenges, as the physical parameters and timing of the fulgurite-generating lightning event still need to be discovered.

Here, we use a unique opportunity from the recent in situ discovery of a natural fulgurite still embedded in its protolith. (The natural fulgurite-generating event is visible in the World Wide Lightning Network data.) Using a high-voltage setup, we further compare this natural fulgurite with the experimentally generated fulgurite obtained from the original protolith. The natural and experimental fulgurites exhibit evidence of similar melting sequences and post-melting recrystallization structures. Using Raman spectroscopy applied to the quartz phase transition, we estimate the thermal gradient present in the fulgurite during formation to be a minimum of 1600 °C at the inner wall of the fulgurite and ca. 600 °C at the outer wall of the fulgurite. Those findings suggest that the current responsible for the cloud-to-ground lightning discharges that generated the natural fulgurite lay in the range of 11 960 to 14 473 kA. The state of the experimental fulgurites matched that of the natural fulgurite, validating the experimental option for studying fulgurite generation.

Keywords: Fulgurite, lightning discharge, experiment, World Wide Lightning Network, Earth Networks Total Lightning Network

INTRODUCTION

Fulgurites are irregular, glassy, tube-shaped formations that occur when lightning discharges (specifically cloud-to-ground or CG) melt the Earth's surface at peak temperatures, followed by rapid cooling. They typically contain a large glass fraction hosting some unmelted, original lithology and often exhibit some quench crystallization.

Only one-third of thundercloud lightning discharges are estimated to reach the ground, potentially generating fulgurites (Rakov 2016). Despite the limited number of examples, it has been proposed that fulgurites may offer valuable data for paleoecology reconstructions (Navarro-González et al. 2007; Ballhaus et al. 2017) and demonstrate the existence of rare essential prebiotic chemical reactants, such as phosphite (e.g., Pasek and Block 2009; Hess et al. 2021; Çalışkanoğlu et al. 2023a; Bindi et al. 2023).

Previous fulgurite research has predominantly focused on natural examples (e.g., Pasek et al. 2012; Ende et al. 2012; Stefanofano et al. 2020; Karadag et al. 2022), with very few experimental studies to date (e.g., Castro et al. 2020; Genareau et al. 2017). Those pioneering experimental studies were severely limited in

their ability to mimic natural lightning due to constraints arising from technical aspects of the experiments, such as the absence of a trigger or a continuing current. They, therefore, largely fail to replicate accurately the conditions of fulgurite petrogenesis. In contrast, the high current and voltage experimental setup (see detail in Çalışkanoğlu et al. 2023b) employed here enables the accurate simulation of lightning discharges responsible for fulgurite formation.

Here, we compare a natural fulgurite (Eastern Turkey) and an equivalent experimentally generated fulgurite obtained using the in situ adjacent protolith as a starting material. The experimental fulgurite, generated under variable, well-controlled experimental conditions, yields new insights into the textural evolution of the natural fulgurite and about temperature gradients during melting and recrystallization at high cooling rates. Simultaneously, we report the first detailed measurements of lightning discharge parameters that we infer led to the formation of the natural fulgurite, thereby effectively constraining the electrical conditions necessary for fulgurite formation.

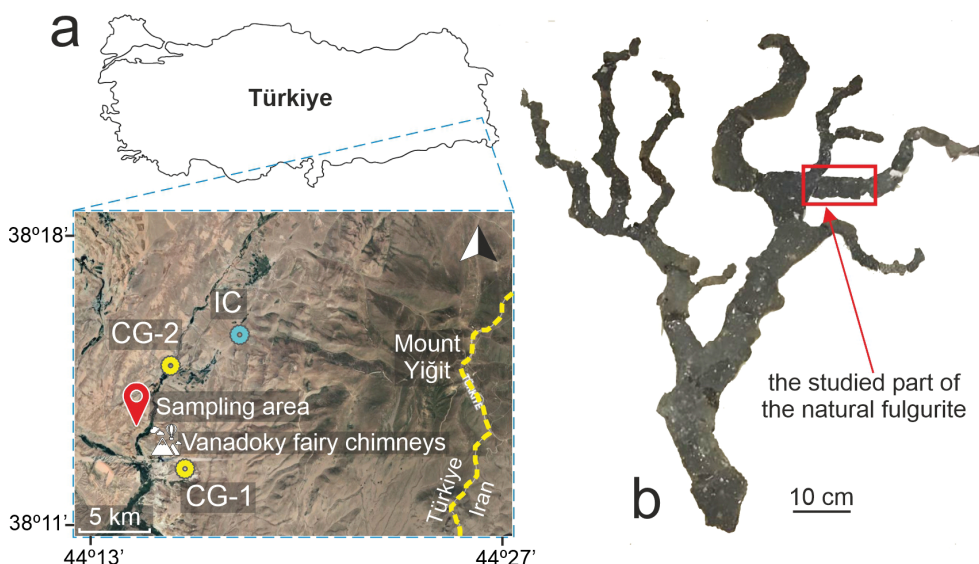
MATERIALS AND METHODS

The natural fulgurite

A sample of natural fulgurite and its adjacent protolith was obtained from a private seller who discovered the fulgurite in northwest Van-Turkey (38°13'17.6"N 44°15'55.9"E) in mid-April 2021 (Figs. 1a and 1b) after a thunderstorm of April 1,

* Corresponding author E-mail: zeynep.caliskanoglu@min.uni-muenchen.de. Orcid <https://orcid.org/0000-0003-3208-810X>

† Open access: Article available to all readers online. This article is CC-BY-NC-ND.



1
2
3
4
5
6
7
8
9
10
11
12
13
14
15
16
17
18
19
20

FIGURE 1. Sampling area and general image of the natural fulgurite. (a) The fulgurite was found northwest of the Vanadoky fairy chimneys in Van, Turkey (Türkiye). The ENTNLN detected two CG and one intracloud (IC) lightning discharges. The topographic image is taken from Google Maps (accessed 2023). (b) A photographic image of the natural fulgurite is shown. The red rectangle indicates the portion of the natural fulgurite object of this study.

2021. The investigated natural fulgurite will be detailed in the Results section below. The CG lightning associated with that thunderstorm was detected by radio-frequency antennas of the Earth Networks Total Lightning Network (ENTLN; Zhu et al. 2022). In addition to the approximate location of the lightning discharge, the antennas provide the magnitude of the current associated with each lightning event. This discovery provides us with a unique opportunity to evaluate natural fulgurite formation vs. experimental fulgurite formation from the protolith using independent control of lightning parameters under realistic laboratory conditions.

The target (protolith) material

The protolith (a soil-bearing epiclastic sediment), collected from an area immediately adjacent to the natural fulgurite (Fig. 1a), was used as a target material for the fulgurite synthesis experiments. The remote location means no nearby communication poles might have accidentally generated the fulgurites artificially (e.g., Kassi et al. 2013).

The local geology consists of several geological units from oldest to youngest: (1) pre-Neogene pyroclastic deposits (pumice, tuff, and ignimbrites) and intermediate (andesite/trachyandesite) deposits from Mount Yiğit (Türkecan 2017); (2) Neogene clastic rocks (conglomerate, sandstone, marl, and, locally, tuff and lava blocks); (3) Pliocene sedimentary deposits (Şenel et al. 1984) and basaltic lava flows, which represent the latest stage of Mount Yiğit volcanism (1.87 ± 0.07 My; Allen et al. 2011). The protolith used as experimental target material was collected from where the Neogene clastic rocks crop out (Fig. 2a).

The protolith appears yellowish-brown and is composed of rock fragments of varying sizes, ranging from ca. 30 μ m to a few centimeters, consisting of mono- and polyminerall grains. The rock fragments exhibit sub-rounded to rounded edges. Energy-dispersive X-ray spectroscopy (EDS) analysis reveals that the monomineralic grains include quartz, plagioclase, and alkali feldspar, along with minor Fe- and Ti-oxides (Figs. 2b–2d). The polyminerall grains exhibit diverse compositions, but plagioclase, quartz, and alkali feldspar are the most common minerals, with minor hornblende, biotite, apatite, zircon, Fe- and Ti-oxides (Figs. 2d and 2e). Most clasts are fully crystalline (Figs. 2e–2g), but some exhibit up to 20% glass (Fig. 2h). Backscattered electron (BSE) images reveal no evidence of lightning-induced effects in the protolith used subsequently as experimental target material.

Sample preparation and analytical techniques

The target material was thoroughly cleaned to remove any potential macroscopic organics (plants). The most comprehensive possible range of macroscopically distinct clasts was selected and roughly crushed to <10 mm, and a mixture

of them was embedded in epoxy for further analytical analyses.

Several 10 mm chips of fulgurites (both natural and experimental) were embedded in their respective epoxy mounts for microtextural analyses.

The surfaces of chips of both natural and experimental fulgurites were examined using a Keyence 3D Laser Scanning Confocal Microscope (LSCM) VK-X1000 with a 5 \times objective lens (WD 22.5) in the Department of Earth and Environmental Sciences at Ludwig-Maximilians-Universität (LMU), Munich, Germany.

BSE images of the target material, natural, and experimental fulgurite samples, were collected using Scanning Electron Microscopy (SEM) at LMU with an accelerating voltage of 20 kV under a low vacuum. Semiquantitative chemical composition data collection at the SEM was conducted through EDS using an Oxford Instrument Aztech software (AztechEnergy Advanced EDS-System) on the natural fulgurite, its protolith, and the experimental fulgurite.

We used the confocal HORIBA Jobin Yvon XploRa micro-Raman spectrometer at the Mineralogical State Collection Munich (SNSB) to identify mineral phases. The instrument was calibrated with a silicon standard, and the spectra were acquired with a green Nd:YAG-Laser (532 nm wavelength), focused through the 100LWD objective lens, with 0.9 μ m laser spot diameter. A grating of 1800 line/mm, a confocal hole of 300 μ m, a slit of 100 μ m, and an exposure time of 30 s combined with three exposures were used. The backscattered Raman radiation was collected between 100–1500 cm^{-1} , with an error of $\pm 1.5 \text{ cm}^{-1}$.

Fulgurite synthesis experiments

We simulated natural lightning discharges in the high voltage laboratory at Universität der Bundeswehr (UniBw) in Germany, utilizing a DC source with a trigger pulse. The setup was designed based on recommendations from the lightning research community, such as the waveforms specified in IEC 62305 (IEC 2010) derived from studies of natural lightning phenomena. For further details regarding the experimental methodology and schematic diagram of the setup, please refer to Çalışkanoğlu et al. (2023b).

The lightning strikes are conducted between two electrodes placed inside a cylindrical sample container, which is connected to an electrical apparatus consisting of two parts: a Marx generator (which produced the trigger pulse) and a DC source (which acted as a prolonged current generator). The container was filled with ~250 g of target material. Initially, the Marx generator generated ca. 135 kA for ca. 100 μ s, creating a conductive path between the electrodes, which were 5.7 cm apart. This high voltage and current initiated the melting of the target material. Subsequently, the DC source was kept constant between ca. 280 and ca. 320 A for ca. 500 ms, simulating the long duration of a natural lightning discharge

21
22
23
24
25
26
27
28
29
30
31
32
33
34
35
36
37
38
39
40
41
42
43
44
45
46
47
48
49
50
51
52
53
54
55
56
57
58
59
60

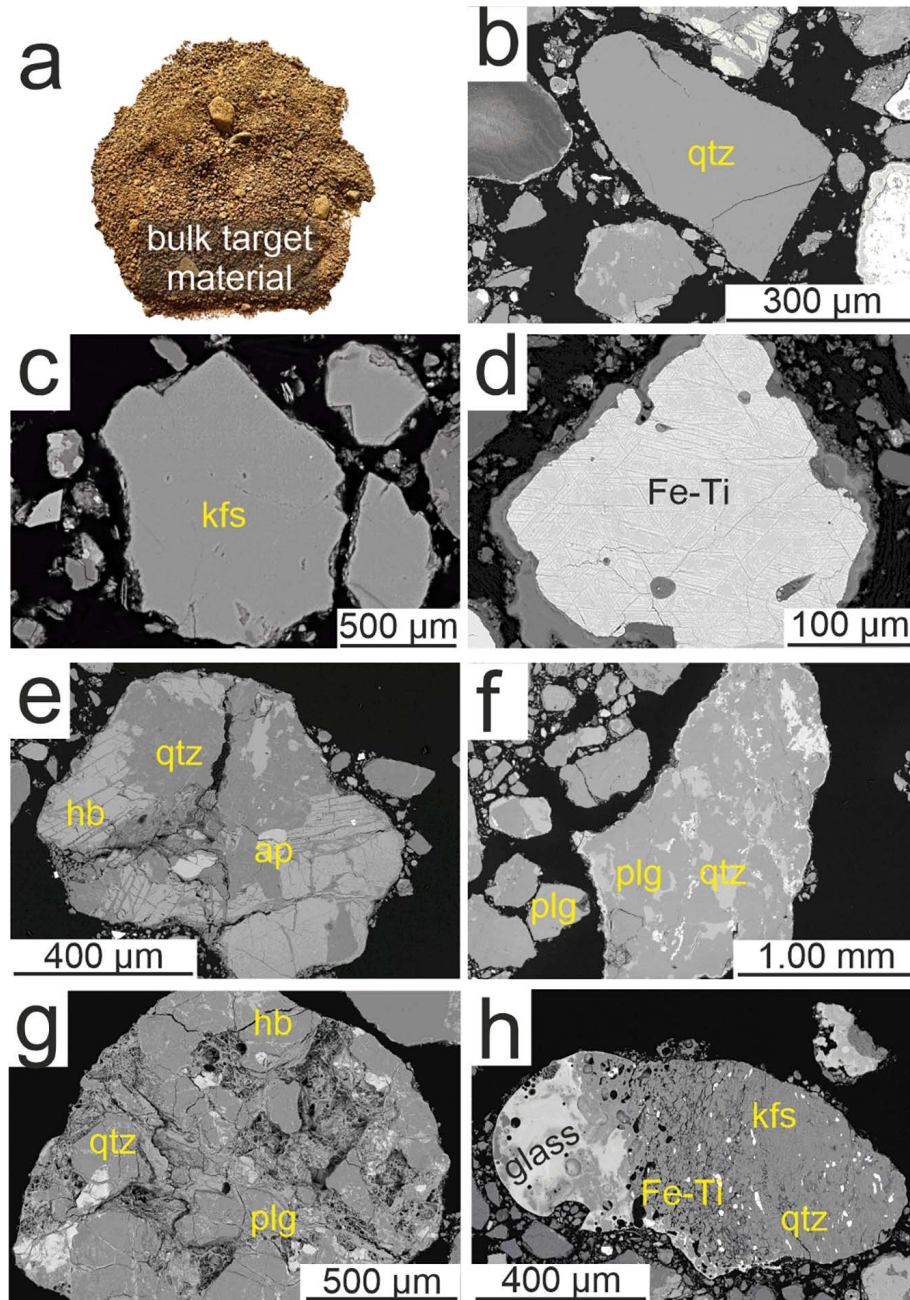


FIGURE 2. Target material and detailed BSE images of its heterogeneous grains. (a) An image of the protolith of natural fulgurite. (b–f) Mono- and polymineralic grains of the target material. These grains represent the sampling area’s clastic rock unit (Şenel et al. 1984). Quartz = qtz; alkali feldspar = kfs; oxides = Fe-Ti; hornblende = hbl; apatite = ap; plagioclase = plg.

(Rakov and Uman 2003; Lapierre et al. 2014). This prolonged current promoted the melting of more material and facilitated the formation of a fulguritic mass.

Several experimental trials were conducted to establish the setup conditions and comprehend the material’s behavior under high current and voltage conditions. All experiments were carried out at atmospheric temperature and pressure. In the first experiment, the target material was utilized in its natural form (fragments ranging from 32 μm to a few centimeters), but no melted pieces or fulguritic structures were observed. Simulated lightning is characterized by a lower peak current than natural lightning, thus preventing larger grains from melting. To ameliorate this discrepancy, ca. 50% of the coarse fraction (>10 mm) was removed, and the experiment was

repeated under the same electrical parameters as above, resulting in the formation of a fulgurite. The waveform of the experimental current was recorded using a Measurement Impulse Analyzer System (MIAS) at an 800–1000 ms time interval.

Field lightning monitoring

The ENTNLN comprises more than 1800 sensors deployed across more than 100 countries, which detect broad-spectrum electric field signals originating from intracloud (IC) and CG lightning events (Liu and Heckman 2011). The CG lightning data are obtained from the World Wide Lightning Location Network (WWLLN) to enhance ENTNLN detection capabilities. The WWLLN detects, locates, and

timestamps lightning strikes worldwide with a spatial accuracy of 10 km and a temporal accuracy of 10 μs (Abreu et al. 2010; Holzworth et al. 2019; Hutchins et al. 2012, 2013; Rodger et al. 2004, 2005). We utilized WWLLN data to identify natural lightning events, which might have generated our natural fulgurite.

We focused on the period of April 1–15, 2021. Our search area was limited to an 8 km radius around the location where the natural fulgurite was found. We detected one IC and two CG lightning events (CG-1 and -2) within the focused area and time frame by using ENTLN data (Table 1; Fig. 1a). IC events do not generate fulgurite; thus, the IC data are neglected in the present study. Both CG-1 and CG-2 lightning strokes showed a “downward negative” direction [the most common for global CG lightning (Rakov and Uman 2003)]. The CGs were ordered according to the time of occurrence, with the location estimates CG-1 and CG-2 illustrated in Figure 1a. It should be noted that due to the technical limitations of the antenna network, the designated locations of the CGs are, within error, equivalent to the fulgurite location [i.e., WWLLN = Rodger et al. (2005); ENTLN = Zhu et al. (2022)]. Considering the data from the WWLLN, we propose that one of these occurrences generated the investigated natural fulgurite.

RESULTS

Natural fulgurite

The natural fulgurite is ca. 112 cm long and ca. 105 cm wide (Fig. 1b). It displays several small branches connected to two main branches. An available piece of this fulgurite was obtained commercially and investigated in the present study (Figs. 3a and 3b). Hereafter, we refer to this sample as the “natural fulgurite.” The natural fulgurite is ca. 17 cm in length and has a diameter of ca. 6 cm. It appears darker than the protolith. The outer surface of the natural fulgurite has a rough texture with several unmelted grains remaining from the protolith (Fig. 2a). In contrast, the central portion of the natural fulgurite is entirely glassy. Vesicles of variable shapes and sizes are present. The “main void” is the largest vesicle (ca. 2.5 cm in size) in the natural fulgurite, as shown in Figure 3b. Immediately adjacent to the

glassy region is a zone of large vesicle concentration. Smaller vesicles are distributed from the glassy region to the unmelted protolith. (Fig. 3c). The fulgurite wall thickness varies from ca. 1 to 3 cm. The fulgurite contains unmelted to partially melted, angular, and sub-angular grains (up to a few millimeters) and a fully melted glassy region. Unmelted grains are common on the outer wall of the fulgurite, whereas partially melted grains are typically scattered in the glassy mass. BSE images show no sharp transition between unmelted and partially melted grains. The glassy mass is composed of a heterogeneous mingling of molten materials (Fig. 3d).

Natural fulgurite grains are mono- and polymineralic, occurring in unmelted and partially melted states. Monomineralic grains are typically alkali feldspar, plagioclase, and quartz or minor Fe- and Ti-oxides. Melts apparently derived from feldspar mingle with the matrix-derived melts, as evidenced by heterogeneity in the glass, in the form of flow structures (Fig. 3d). Partially melted quartz crystals are commonly fractured (Fig. 3e). The phase change from α-quartz (crystals located in the outer zone of the fulgurite) to cristobalite (crystals located close to the inner wall) was also detected.

Post-melting recrystallization structures with different compositions were detected, as shown in Table 2. No orientation is apparent in the growth pattern of these structures. Their size reaches a maximum of 1 mm. Prismatic-tabular structures are observed, which are enriched in SiO₂, Al₂O₃, CaO, and Na₂O (Fig. 3f). Skeletal structures are observed, which are enriched in MgO (Fig. 3g). Other structures (i.e., cross, spherical, and another skeletal) have notably high FeO contents (Figs. 4a–4c). The cross and spherical structures are found in proximity to one another and appear to be formed sequentially. These structures’ considerably smaller size (<1 μm) prevents accurate composition measurements because of SiO₂ and Al₂O₃ contamination from the surrounding material. However, their compositions appear similar to those of the Fe-containing phases.

The polymineralic grains in the natural fulgurite consist mainly of quartz, plagioclase, and alkali feldspar, with minor

TABLE 1. WWLLN data around the sampling area of the natural fulgurite

Type of lightning	Date	Time	Location	Peak current (kA)	IC height (km)	Number sensors
IC	01.04.20	12:25:32	38°15'01.2"N 44°18'32.7"E	5.113	18.917	5
CG-1	01.04.20	17:27:14	38°11'04.6"N 44°17'19.3"E	-14.473	0	6
CG-2	01.04.20	17:29:41	38°14'22.2"N 44°16'47.3"E	-11.960	0	5

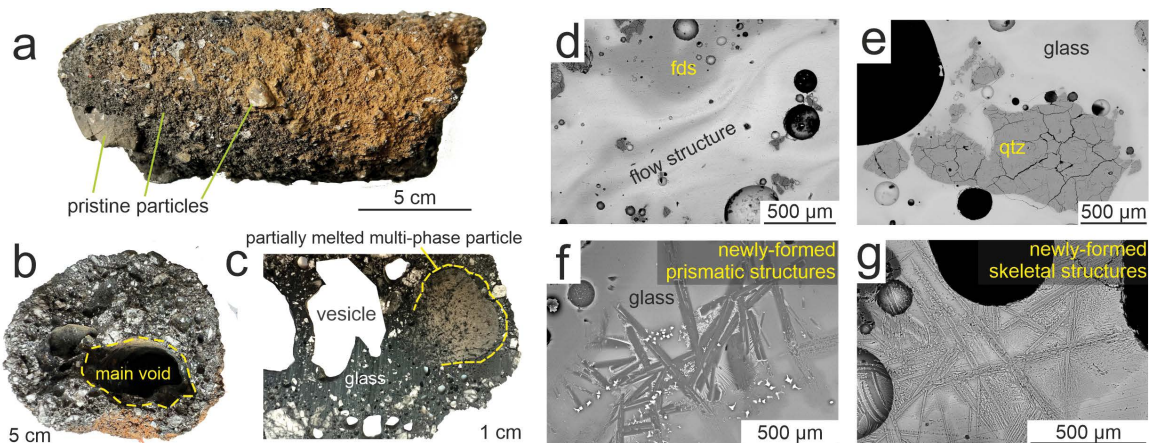


FIGURE 3. Detailed optical and BSE images of the natural fulgurite. (a) A photo of the studied part of the fulgurite specimen in detail. (b) A section view of the natural fulgurite exhibits the “main void.” (c) An optical image of a segment of a section of the natural fulgurite captured by 3D LSCM, showing vesicles of varying sizes and shapes. (d) The heterogeneous glass mass displays a flow structure within the glass mass. (e) BSE images reveal fractured quartz crystals. (f) Newly formed prismatic-tabular structures exhibit enrichment in SiO₂, Al₂O₃, Na₂O, and K₂O. (g) Newly formed skeletal structures present MgO enrichment. Feldspar = fds.

TABLE 2. Chemical composition of natural and experimental fulgurites (SEM-EDS normalized data)

Natural fulgurite										
	Glass mass	Melting morphologies of feldspar				Post-melting recrystallization structures				
		Solid		Vesiculated	Molten	Fe-rich phases			Prismatic-tabular	Mg-rich skeletal
		Plagioclase	Alkali feldspar			Cross	Spherical	Skeletal		
Si ₂ O	60.11	66.07	64.69	67.24	69.21	57.31	42.29	3.60	56.89	54.07
Al ₂ O ₃	17.01	21.45	18.82	20.76	17.41	13.50	11.45	2.12	25.94	4.89
FeO	9.91	0.17	0.14	0.19	2.99	22.92	35.21	91.23	2.14	12.76
CaO	3.29	1.85	0.06	0.69	1.95	0.78	0.81	0.01	8.63	2.22
K ₂ O	2.61	0.96	14.63	3.53	3.30	0.37	0.31	0.02	0.60	0.36
Na ₂ O	3.09	9.31	1.58	7.35	3.63	2.41	4.16	0.18	5.13	0.56
MgO	2.49	0.1	0.02	0.09	1.20	1.63	2.02	0.50	0.34	24.19
TiO ₂	1.26	0.04	0.02	0.03	0.24	1.01	3.15	1.86	0.22	0.47
MnO	0.19	0.02	0.01	0.03	nd	0.05	0.13	0.03	0.04	0.28
Cr ₂ O ₃	0.04	nd	0.02	0.02	nd	0.02	0.02	0.06	0.07	0.02
W	nd	nd	nd	nd	nd	nd	0.45	0.19	nd	0.09
Cu	nd	0.03	0.01	nd	0.08	nd	nd	0.02	nd	nd

Experimental fulgurite											
	Glass mass	Melting morphologies of feldspar				Post-melting recrystallization structures					
		Solid		Vesiculated	Molten	Fe-rich phases			Structure 1	Structure 2	Structure 3
		Plagioclase	Alkali feldspar			Structure 1	Structure 2	Structure 3			
Si ₂ O	64.11	65.48	63.77	66.07	63.98	21.53	21.61	42.07			
Al ₂ O ₃	17.78	21.87	18.89	19.14	24.42	nd	8.31	14.42			
FeO	6.71	0.92	0.24	2.35	0.38	77.13	65.26	31.52			
CaO	3.57	0.65	0.07	0.52	0.88	nd	1.26	1.73			
K ₂ O	1.91	1.94	16.68	8.05	2.82	0.07	0.42	1.94			
Na ₂ O	2.28	8.38	0.22	3.27	7.20	1.12	0.80	2.33			
MgO	1.52	0.31	0.08	0.5	0.16	nd	1.03	2.78			
TiO ₂	1.18	0.10	nd	nd	nd	0.04	1.04	2.98			
MnO	0.11	0.25	0.02	nd	0.39	nd	0.08	0.20			
Cr ₂ O ₃	nd	0.10	nd	nd	0.55	0.10	0.17	nd			
W	0.72	0.35	nd	nd	0.06	0.01	nd	nd			
Cu	nd	nd	0.03	0.01	0.10	nd	0.04	nd			

biotite, hornblende, apatite, zircon, and oxides (Fe and Ti). These grains are found in both unmelted and partially melted regions. The volume fraction of unmelted grains is much lower than that of partially melted grains in the glassy region. Feldspar crystals exhibit three morphologies: “solid,” “vesiculated,” and “molten.” The solid morphology represents the feldspar crystals (either

alkali feldspar or plagioclase) that do not show any chemical and physical changes (i.e., unmelted) (Fig. 4d). These crystals are only found in the outer wall of the natural fulgurite. The vesiculated morphology indicates crystals containing mainly rounded vesicles (Fig. 4e). They are mostly found in the middle of the natural fulgurite wall. The chemical composition of this region

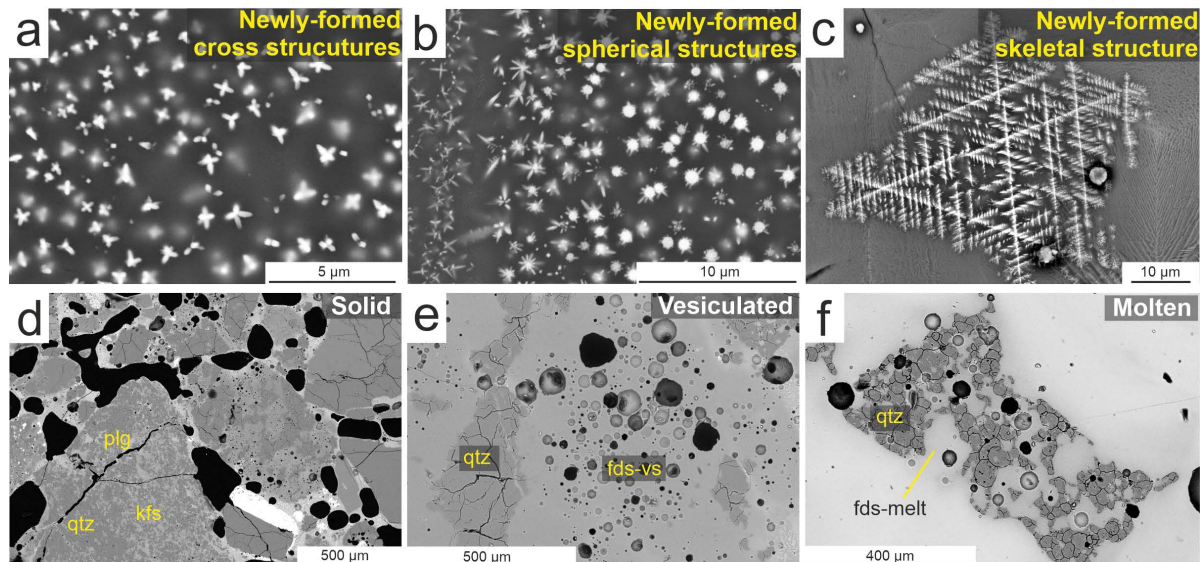


FIGURE 4. Post-melting recrystallization structures and melting morphologies of the main crystals (feldspar) in the natural fulgurite are shown in a–c and d–f, respectively. Fe-rich recrystallization structures grew in different forms, such as cross (a), spherical (b), and skeletal (c). (d) Unmelted polyminerals grains are named “solid.” (e) Feldspar displays vesicles due to high-temperature interactions in the “vesiculated.” (f) The “molten” exhibits complete melting of the feldspar. Vesicle = vs.

is enriched in SiO₂, Al₂O₃, Na₂O, and K₂O. The Na₂O and K₂O values are variable depending on the volume ratio of plagioclase and alkali feldspar in the primary grains. The molten morphology may result from feldspar crystals melting completely in the presence of some other minor phases, such as Fe-oxide (Fig. 4f).

Experimental fulgurite

The experimentally generated fulgurite is also tube-like without branches (Fig. 5a) and appears dark brown. It is ~7 cm in length and 1 cm in width, with a main void diameter of ~7 mm (Fig. 5b). The thickness of the fulgurite wall is ca. 2 mm. The distribution of unmelted and partially melted grains, as well as the glassy region, is found to be quite similar to that of the natural fulgurite, and there is no sharp transition between unmelted and partially melted grains at the outer edge of the experimental fulgurite. However, the proportion of the unmelted grains in the glassy region is much lower than in the natural fulgurite, presumably due to the finer grain size of the target material. The average grain size of both the unmelted and partially melted grains is ~0.5 mm. Several vesicles, ranging up to 1 mm in size (rounded and sub-rounded), are highly concentrated between unmelted and partially melted regions (Fig. 5c).

The experimental fulgurite contains mono- and polymineralic grains in both unmelted and partially melted forms. Quartz and feldspar crystals are the two monomineralic grains. Feldspar

crystals are mingled in the glassy region, resulting in the observed flow structures (Fig. 5d). Quartz crystals are ca. 0.5 mm in size (Fig. 5e), and they exhibit physical deformation such as fractures (Fig. 5f) and have been identified as α-quartz via Raman spectroscopic analysis.

Three distinct post-melting recrystallization structures are observed. They are numbered 1, 2, and 3 based on their structural differences from right to left on the BSE image (Fig. 5g). They exhibit strong FeO enrichment together with high SiO₂ and Al₂O₃ contents (Table 2). Structure 1 displays a cross shape, as observed in the natural fulgurite (Fig. 4a). In structure 2, radial arms extend from a central point to form spherulites. Structure 3 displays a symmetric skeletal form. The structures 1 and 3 cover a larger area of the fulgurite than the structure 2. Analysis of these small, Fe-rich structures suffers from contamination (i.e., SiO₂ and Al₂O₃) originating from the surrounding glass.

The polymineralic grains consist mainly of quartz, plagioclase, and alkali feldspar with hornblende, apatite, and minor Fe-Ti oxides. These minor phases are solely detected in the partially melted grains near the outer wall of the experimental fulgurite. Quartz crystals have retained their general form with numerous fractures and show no notable chemical changes. In contrast, feldspars exhibit chemical and mechanical changes. They show the same textural morphologies (solid, vesiculated, and molten) (Figs. 5h–5j) as described for the natural fulgurite

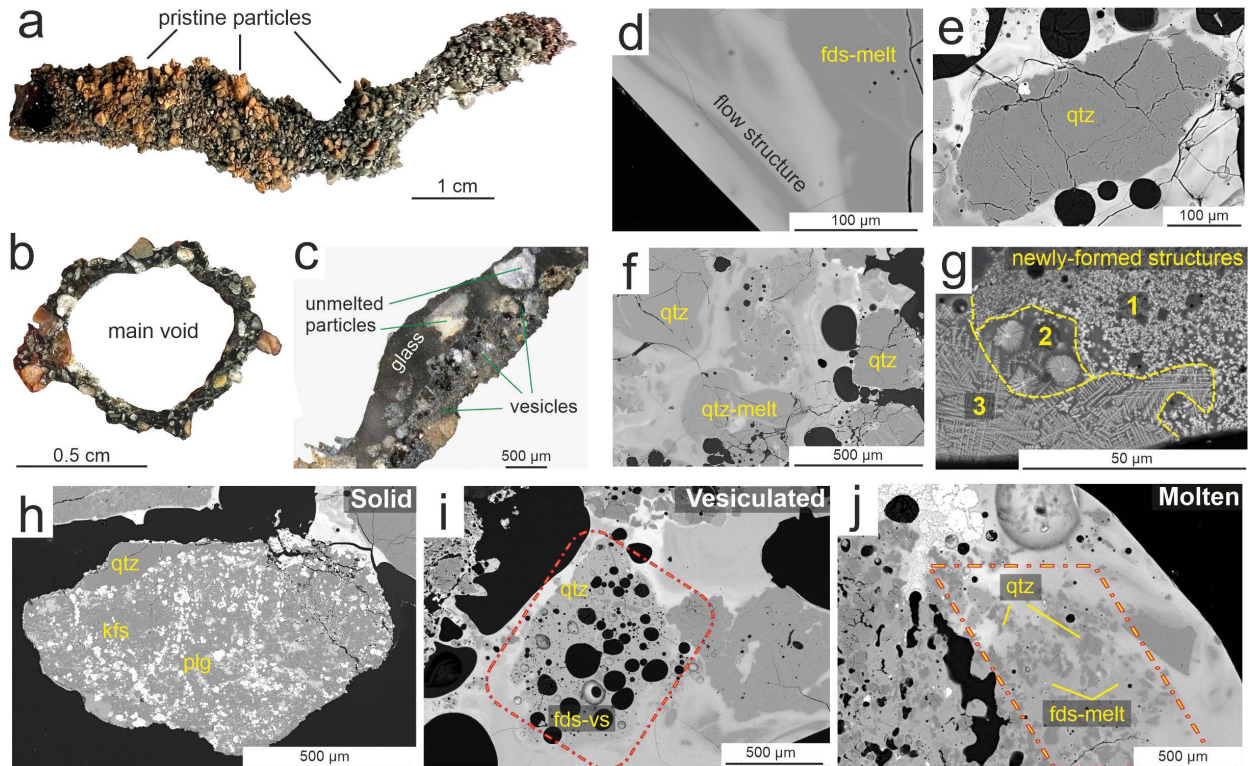


FIGURE 5. Optical and BSE images of the experimental fulgurite. (a) A photo of the experimentally generated fulgurite. (b) A sectional view of the experimental fulgurite. (c) An optical image of the fulgurite shows unmelted and partially melted mono- and polymineralic grains in a glassy mass. (d) Partially melted feldspar crystals, which have mingled with the glass mass. (e) A BSE image of a monomineralic partially melted quartz. (f) Partially melted quartz and alkali feldspar crystals. (g) Newly formed structures grew in different forms (i.e., spherical and skeletal). The feldspar crystals exhibit a “solid” (h), “vesiculated” (i), and “molten” morphologies (j) in the polymineralic grains.

(Figs. 4d–4f). Feldspar crystals (alkali feldspar and plagioclase) in the solid morphology are detected in the outer wall of the experimental fulgurite (Fig. 5h). They exhibit enhanced vesiculation (Fig. 5i). In the molten morphology, feldspars appear entirely molten without any recognizable morphological crystal form close to the interior fulgurite wall, and they are surrounded by fractured quartz crystals (Fig. 5j). EDS measurements on the well-mixed glassy region indicate that the glass composition of the experimental fulgurite is quite similar to that of the natural fulgurite (Table 2).

DISCUSSION

Fulgurite was experimentally generated from the protolith recovered adjacent to a natural fulgurite. The formation of a fulgurite is confirmed to be a complex process that depends on several factors, including the lightning parameters (i.e., temperature and current), as well as the composition and the state of the host rock. Even though the current intensities of the natural lightning discharge, ca. $13\,000 \pm 1.250$ kA (Table 1), and the experiment, ca. 300 A are vastly different, our results reveal that the fulgurites generated in nature and experiments resemble each other closely. A notable exception is that the higher natural current does lead to a higher degree of melting of coarser grains. A possible explanation for this scale-invariant character may lie in the intrinsic fractal nature of lightning discharges (Niemeyer et al. 1984; Wisemann and Zeller 1986). Previous work from Çalışkanoğlu et al. (2023b) indicates that the continuing current of a lightning strike has a noticeable effect on the formation of fulgurite, indicating a threshold of ca. 100 ms for fulgurite formation. We confirm here that a 300 A current and a prolonged duration of discharge (ca. 100 ms) facilitates the formation of fulgurite from the silicate protolith (Maurer 2021), as it has been previously demonstrated for non-silicate (Çalışkanoğlu et al. 2023a) protolith.

Temperature gradients and grain size distribution both exert first-order influences on fulgurite texture. The temperature of natural lightning discharges typically ranges between 10 000 to 28 000 K (Paxton et al. 1986). Based on melting temperatures, we observe that our simulated lightning discharge generates a minimum of ca. 2000 K (Çalışkanoğlu et al. 2023a, 2023b). Regions experiencing lower temperatures, due to their distal location to the lightning plasma and higher concentration of coarse grain sizes, exhibit a higher proportion of partially melted and unmelted grains in the fulgurite, yielding distinct regions whose textures are systematically defined by their degrees of melting (e.g., Hess et al. 2021; Kenny and Pasek 2021; Çalışkanoğlu et al. 2023a, 2023b). In both nature and experiment, coarse grains that have been partially melted exhibit distinctive flow structures in their glassy products, indicating that such melts are not homogenized during fulgurite formation (cf. Lavallée et al. 2015). In contrast, the homogeneous glassy (fully remelted) regions of experimental and natural fulgurites exhibit similar chemistry as determined by SEM/EDS (Table 2).

Quartz crystals (initially both mono- and polymineralic grains) undergo a phase change (Figs. 6a and 6b) with increasing temperature, resulting in a fractured structure. Folstad et al. (2023) indicate that cracks in quartz are commonly observed in two temperature ranges. The first range, ~ 300 – 600 °C, primarily arises from volume changes in impurity regions, uneven surfaces

of quartz, and/or the presence of fluid inclusions. The second range, ca. 1300 – 1600 °C, is likely a consequence of the phase transformation of quartz from β -quartz to β -cristobalite. As noted above, the natural fulgurite exhibits α -quartz in the outer wall and β -cristobalite in the inner wall. This implies the presence of a strong temperature gradient across ca. 1 cm. In contrast, the experimental fulgurite exhibits no cristobalite. Possible reasons for this discrepancy include: (1) the simulated lightning may not have reached the equivalent temperature range and/or (2) the pressure generated by simulated lightning may be lower than

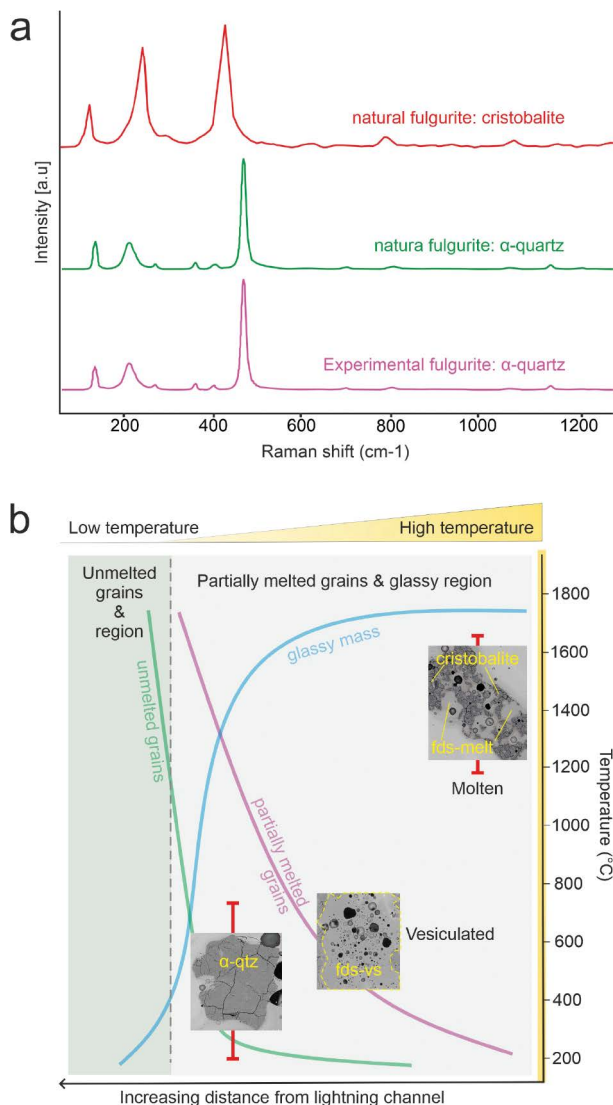


FIGURE 6. Micro-Raman spectroscopy of quartz crystals and a schematic diagram illustrating the evolution of grains in the fulgurites. (a) The Raman spectra of quartz crystals in fulgurites from each fulgurite's inner and outer walls. The experimental fulgurite exhibits only α -quartz, and natural fulgurite displays both α -quartz and cristobalite. (b) The textural evolution of the fulgurites concerning temperature development during lightning discharge. The textural evolution among the defined morphologies (i.e., solid, vesiculated, and molten) is scaled in temperature using the α - β transition (Folstad et al. 2023) and cristobalite stability (Wagstaff 1969).

the natural lightning.

Feldspar crystals situated in proximity to the lightning plasma undergo complete melting, whereas those subjected to lower temperatures display partial melting with vesicle formation. This distinction within the feldspar crystals supports the strong temperature gradient extending from the inner wall (adjacent to the plasma) to the outer wall of the fulgurite.

Upon cooling, both the natural and experimental fulgurites reveal the presence of multiple coexisting crystalline structures (i.e., spherical and dendritic) (Figs. 3f, 3g, 4a–4c, and 5g). Similar crystal structures have also been reported in other rapidly quenched glasses, such as impactites, meteorites, and chondrules (e.g., Kumler and Day 2021). Skeletal structures (magnetite) have been previously documented in fulgurites by Ablesimov et al. (1986) and Grapes and Müller-Sigmund (2010). To the best of our knowledge, this study marks the first documented occurrence of spherical Fe-rich forms within natural and experimental fulgurites. The juxtaposition of distinct growth patterns and crystal sizes might reflect locally varying melt compositions and/or different cooling rates determined by proximity to the lightning plasma and heterogeneous composition.

IMPLICATIONS

This work demonstrated a realistic comparison between natural and experimental fulgurites for the first time, revealing a remarkable similarity in their textural and mineralogical evolution. This validates that the state of the experimental fulgurite matched that of the natural fulgurite using the DC source trigger-pulse setup as a lightning simulator. This work also further documents the physical parameters (maximum voltage and current) of lightning strikes that likely generated the natural fulgurite. Our results interestingly suggest a scale-invariant character of the experimental fulgurites concerning the natural ones, whereby the lower voltage and current values used in the experiments allow the reproduction of identical textures observed in the natural fulgurite. As shown in previous experiments, we confirm the importance of long-duration (hundreds of milliseconds) continuous currents for generating extensive melting and, ultimately, fulgurite formation. This work introduces a novel methodology for reproducible fulgurite generation through laboratory experiments. This opens up possibilities for systematic petrogenetic analysis of fulgurite formation with broader geological implications, providing researchers with a controlled environment to explore and understand the processes involved.

ACKNOWLEDGMENTS AND FUNDING

The authors thank Jeff Lapierre for providing the ENTLN dataset. The authors thank Philippe Schmitt-Kopplin for his assistance and technical support and Daniel Weidendorfer for useful discussions and advice. They thank Associate Editor Kate Kiseeva for her careful guidance and two reviewers (Christopher J. Stefano and an anonymous) for their thorough reviews. The research was financially supported by the Volkswagen Foundation (VW Stiftung) under Project-ID 94809. D.B.D. acknowledges ERC 2018 ADV Grant 834255 (EAVESDROP), and C.C. acknowledges ERC 2019 COG Grant 864052 (VOLTA).

REFERENCES CITED

Ablesimov, N.Y., Tsyurupa, A.I., and Lipatov, V.G. (1986) Phase and element ratios upon fulguritization of basalt. *Transactions (Doklady) of the USSR Academy of Sciences, Earth Science Section*, 290, 161–164.

Abreu, S.F., Chandan, D., Holzworth, R.H., and Strong, K. (2010) A performance assessment of the World Wide Lightning Location Network (WWLLN) via comparison with the Canadian Lightning Detection Network (CLDN).

Atmospheric Measurement Techniques, 3, 1143–1153, <https://doi.org/10.5194/amt-3-1143-2010>.

Allen, B.M., Mark, F.D., Kheirkhah, M., Barfod, D., Emami, H.M., and Saville, C. (2011) $^{40}\text{Ar}/^{39}\text{Ar}$ dating of Quaternary lavas in northwest Iran: Constraints on the landscape evolution and incision rates of the Turkish-Iranian plateau. *Geophysical Journal International*, 185, 1175–1188, <https://doi.org/10.1111/j.1365-246X.2011.05022.x>.

Ballhaus, C., Wirth, R., Fonseca, R.O.C., Blanchard, H., Pröll, W., Bragagni, A., Nagel, T., Schreiber, A., Dittrich, S., Thome, V., and others. (2017) Ultra-high pressure and ultra-reduced minerals in ophiolites may form by lightning strikes. *Geochemical Perspectives Letters*, 5, 42–46, <https://doi.org/10.7185/geochemlet.1744>.

Bindi, L., Feng, T., and Pasek, M.A. (2023) Routes to reduction of phosphate by high-energy events. *Communications Earth & Environment*, 4, 70, <https://doi.org/10.1038/s43247-023-00736-2>.

Çalışkanoğlu, A.Z., Dingwell, D.B., Cimarelli, C., Camara, A.S.B., Breitzke, H., Buntkowsky, G., Pasek, M.A., Braun, D., Scheu, B., and Molaverdikhani, K. (2023a) Reactive phosphorus via simulated lightning discharge: A role for fulgurites in prebiotic chemistry. *Chemical Geology*, 620, 121343, <https://doi.org/10.1016/j.chemgeo.2023.121343>.

Çalışkanoğlu, A.Z., Camara, A.S.B., Cimarelli, C., Dingwell, D.B., and Hess, K.U. (2023b) Experimental generation of fulgurite under realistic lightning discharge conditions. *Scientific Reports*, 13, 11685, <https://doi.org/10.1038/s41598-023-38781-8>.

Castro, J.M., Keller, F., Feisel, Y., Lanari, P., Helo, C., Mueller, S.P., Schipper, C.I., and Thomas, C. (2020) Lightning-induced weathering of Cascadian volcanic peaks. *Earth and Planetary Science Letters*, 552, 116595, <https://doi.org/10.1016/j.epsl.2020.116595>.

Ende, M., Schorr, S., Kloess, G., Franz, A., and Tovar, M. (2012) Shocked quartz in Sahara fulgurite. *European Journal of Mineralogy*, 24, 499–507, <https://doi.org/10.1127/0935-1221/2012/0024-2188>.

Folstad, M.A., Yu, H., Wang, H., and Tangstad, M. (2023) Disintegration of six different quartz types during heating to 1600 °C. *Minerals*, 13, 132, <https://doi.org/10.3390/min13020132>.

Genareau, K., Gharghabi, P., Gafford, J., and Mazzola, M. (2017) The elusive evidence of volcanic lightning. *Scientific Reports*, 7, 15508, <https://doi.org/10.1038/s41598-017-15643-8>.

Grapes, R.H. and Müller-Sigmund, H. (2010) Lightning-strike fusion of gabbro and formation of magnetite-bearing fulgurite, Cornone di Blumone, Adamello, Western Alps, Italy. *Mineralogy and Petrology*, 99, 67–74, <https://doi.org/10.1007/s00710-009-0100-3>.

Hess, B.L., Piazzolo, S., and Harvey, J. (2021) Lightning strikes as a major facilitator of prebiotic phosphorus reduction on early Earth. *Nature Communications*, 12, 1535, <https://doi.org/10.1038/s41467-021-21849-2>.

Holzworth, R.H., McCarthy, M.P., Brundell, J.B., Jacobson, A.R., and Rodger, C.J. (2019) Global distribution of superbolts. *Journal of Geophysical Research: Atmospheres*, 124, 9996–10005, <https://doi.org/10.1029/2019JD030975>.

Hutchins, M.L., Holzworth, R.H., Rodger, C.J., and Brundell, J.B. (2012) Far-field power of lightning strokes as measured by the World Wide Lightning Location Network. *Journal of Atmospheric and Oceanic Technology*, 29, 1102–1110, <https://doi.org/10.1175/JTECH-D-11-00174.1>.

Hutchins, M.L., Jacobson, A.R., Holzworth, R.H., and Brundell, J.B. (2013) Azimuthal dependence of VLF propagation. *Journal of Geophysical Research: Space Physics*, 118, 5808–5812, <https://doi.org/10.1002/jgra.50533>.

IEC (2010) IEC 62305-1:2010—Protection against lightning—Part 1: General Principles (2nd ed.), 137 p. International Electrotechnical Commission.

Karadag, A., Kaygisiz, E., Nikitin, T., Ongen, S., Ogruc Ildiz, G., Aysal, N., Yilmaz, A., and Fausto, R. (2022) Micro-Raman spectroscopy and X-ray diffraction analyses of the Core and shell compartments of an iron-rich fulgurite. *Molecules (Basel, Switzerland)*, 27, 3053, <https://doi.org/10.3390/molecules27103053>.

Kassi, A.M., Kasi, A.K., Friis, H., and Kakar, D.M. (2013) Occurrences of rock fulgurites associated with steel pylons of the overhead electric transmission line at Tor Zawat, Ziarat District and Jang Tor Ghar, Muslim Bagh, Pakistan. *Turkish Journal of Earth Sciences*, 22, 1010–1019, <https://doi.org/10.3906/yer-1207-6>.

Kenny, G.G. and Pasek, M.A. (2021) The response of zircon to the extreme pressures and temperatures of a lightning strike. *Scientific Reports*, 11, 1560, <https://doi.org/10.1038/s41598-021-81043-8>.

Kumler, B. and Day, J.M.D. (2021) Trace element variations generated by magmatic and post-crystallization processes in eucrite meteorites. *Geochimica et Cosmochimica Acta*, 301, 211–229, <https://doi.org/10.1016/j.gca.2021.03.002>.

Lapierre, J.L., Sonnenfeld, R.G., Edens, H.E., and Stock, M. (2014) On the relationship between continuing current and positive leader growth. *Journal of Geophysical Research: Atmospheres*, 119, 12,479–12,488, <https://doi.org/10.1002/2014JD022080>.

Lavallée, Y., Hirose, T., Kendrick, J.E., Hess, K.U., and Dingwell, D.B. (2015) Fault rheology beyond frictional melting. *Proceedings of the National Academy of Sciences of the United States of America*, 112, 9276–9280, <https://doi.org/10.1073/pnas.1413608112>.

- 1 Liu, C., and Heckman, S. (2011) The application of total lightning detection and
 2 cell tracking for severe weather prediction. In Proceedings of the 91st American
 3 Meteorological Society Annual Meeting, Seattle, Washington, U.S.A. 23–27.
 4 American Meteorological Society.
- 5 Maurer, B. (2021) Lightning induced olivine spherules. Experimental generation
 6 and structural and chemical characterization of crystalline and glassy particles
 7 generated by artificial lightning, 71 p. M.S.c. thesis, Ludwig-Maximilians-
 8 Universität.
- 9 Navarro-González, R., Mahan, S.A., Singhvi, A.K., Navarro-Aceves, R., Rajot,
 10 J-L., McKay, C.P., Coll, P., and Raulin, F. (2007) Paleocology reconstruction
 11 from trapped gases in a fulgurite from the late Pleistocene of the Libyan Desert.
 12 *Geology*, 35, 171–174, <https://doi.org/10.1130/G23246A.1>.
- 13 Niemeyer, L., Pietronero, L., and Wiesmann, H.J. (1984) Fractal dimension
 14 of dielectric breakdown. *Physical Review Letters*, 52, 1033–1036, <https://doi.org/10.1103/PhysRevLett.52.1033>.
- 15 Pasek, M.A. and Block, K. (2009) Lightning-induced reduction of phosphorus oxida-
 16 tion state. *Nature Geoscience*, 2, 553–556, <https://doi.org/10.1038/ngeo580>.
- 17 Pasek, M.A., Block, K., and Pasek, V. (2012) Fulgurite morphology: A classification
 18 scheme and clues to formation. *Contributions to Mineralogy and Petrology*,
 19 164, 477–492, <https://doi.org/10.1007/s00410-012-0753-5>.
- 20 Paxton, A.H., Gardner, R.L., and Baker, L. (1986) Lightning return stroke: A
 21 numerical calculation of the optical radiation. *The Physics of Fluids*, 29,
 22 2736–2741, <https://doi.org/10.1063/1.865514>.
- 23 Rakov, V.A. (2016) *Fundamentals of Lightning*, 248 p. Cambridge University Press.
- 24 Rakov, V.A. and Uman, M.A. (2003) *Lightning: Physics and Effects*, 700 p.
 25 Cambridge University Press.
- 26 Rodger, C.J., Brundell, J.B., Dowden, R.L., and Thomson, N.R. (2004) Location
 27 accuracy of long distance VLF lightning location network. *Annales Geophy-
 28 sicae*, 22, 747–758, <https://doi.org/10.5194/angeo-22-747-2004>.
- 29 Rodger, C.J., Brundell, J.B., and Dowden, R.L. (2005) Location accuracy of VLF
 30 World Wide Lightning Location (WWLL) network: Postalgorithm upgrade.
 31 *Annales Geophysicae*, 23, 277–290, <https://doi.org/10.5194/angeo-23-277-2005>.
- 32 Şenel, M., Acarlar, M., Çakmakoğlu, A., Dağ, Z., Erkanol, D., Özçen, S.,
 33 Taşkiran, M.A., Ünal Ulu, M.F., and Yıldırım, H. (1984) Özalp (Van)-İran
 34 sınırı arasındaki alanın jeolojisi. Maden Tetkik ve Arama Genel Müdürlüğü
 35 Rapor No: 7623, Ankara, unpublished.
- 36 Stefano, C.J., Hackney, S.A., and Kampf, A.R. (2020) The occurrence of iron sili-
 37 cides in a fulgurite: Implications for fulgurite genesis. *Canadian Mineralogist*,
 38 58, 115–123, <https://doi.org/10.3749/canmin.1900019>.
- 39 Türkecan, A. (2017) İran sınırında bir volkan—Yığıt dağı. MTA Doğal Kaynaklar
 40 ve Ekonomi Bülteni, 23, 77–86.
- 41 Wagstaff, F.E. (1969) Crystallization and melting kinetics of cristobalite.
 42 *Journal of the American Ceramic Society*, 52, 650–654, <https://doi.org/10.1111/j.1151-2916.1969.tb16069.x>.
- 43 Wiesmann, H.J. and Zeller, H.R. (1986) A fractal model of dielectric breakdown and
 44 pre-breakdown in solid dielectrics. *Journal of Applied Physics*, 60, 1770–1773,
 45 <https://doi.org/10.1063/1.337219>.
- 46 Zhu, Y., Stock, M., Lapierre, J., and DiGangi, E. (2022) Upgrades of the Earth
 47 networks total lightning network in 2021. *Remote Sensing (Basel)*, 14, 2209,
 48 <https://doi.org/10.3390/rs14092209>.

MANUSCRIPT RECEIVED SEPTEMBER 14, 2023

MANUSCRIPT ACCEPTED JANUARY 31, 2024

ACCEPTED MANUSCRIPT ONLINE FEBRUARY 7, 2024

MANUSCRIPT HANDLED BY KATE KISEEVA